JOURNAL OF DEFENCE AND SECURITY INDUSTRY

*Journal of Defence and Security Industries: Strategy and Technology*, 2026, 1(1)

Science & Technology Section

# Comprehensive Investigation of Static and Fatigue Performance of Fiber Bragg Grating, Digital Image Correlation and Strain Gages

Şahin Gören [1], Salim Çalışkan [1,*]

## Abstract

In contemporary practice, a significant application of strain gauges lies in the experimental stress analysis of structural components, particularly within the aerospace sector. However, over the last two decades, fiber optic sensors, particularly Fiber Bragg Grating (FBG) sensors, have been successfully utilized for strain measurements, gaining recognition for their dependable performance. These sensors deliver strain measurement precision that rivals traditional methods such as strain gauges and extensometers. A major advantage of FBG sensors over electrical strain gauges lies in their long-term stability. Additionally, FBG sensors support multiplexing, meaning several sensors can be placed on a single fiber, enabling the collection of multiple simultaneous measurements including the detection of strain, pressure, temperature, and vibration signals. Nevertheless, FBG and conventional techniques also exhibit similar features: they provide localized, directional measurements, require temperature compensation, and are often applied by bonding them to the surface of structures. Digital Image Correlation (DIC), on the other hand, is a non-contact optical method that measures full-field surface geometry, displacement, and strain using digital cameras. DIC is especially useful for monitoring structures by taking periodic images and determining strain and displacement over time or under various operating conditions. While traditional tools such as resistive strain gauges are frequently used in testing composite materials, they come with certain challenges. These include bonding and surface preparation difficulties, the need for direct surface contact and providing only single-point data. While DIC provides a broader measurement capability, its precision depends heavily on the quality of the calibration process and the testing conditions. This study investigates the experimental assessment of strain through the application of traditional strain gauges, FBG sensors, and DIC methodologies on glass fiber reinforced composite (GFRC) laminate coupon specimens subjected to quasi-static and constant amplitude fatigue loading. The work aims to comparatively investigate the sensitivity of optical fiber sensors, strain gauges and DIC.

**Keywords:** Fiber Bragg Grating, strain gage, digital image correlation, mechanical testing, composite.

Received: 14.11.2025 Accepted: 24.12.2025 Research Article

[1] Turkish Aerospace Industries Inc., Ankara, Türkiye

* Corresponding author.

✉ salim.caliskan@tai.com.tr

**Cite this article as:** Gören, S., & Çalışkan, S. (2026). Comprehensive investigation of static and fatigue performance of Fiber Bragg Grating, digital image correlation and strain gages. *Journal of Defence and Security Industry: Strategy and Technology 1*, 140-153.

## 1. Introduction

Although Digital Image Correlation (DIC), Fiber Bragg Grating (FBG) sensors, and strain gauges are widely utilized in experimental mechanics, most existing studies primarily emphasize their individual strengths and weaknesses, often neglecting a holistic comparison under diverse and complex loading scenarios. This study seeks to address this shortcoming by conducting a systematic evaluation of these techniques, focusing on their performance, comparative error assessment, and practical utility. By doing so, it provides valuable insights to inform the selection of the most suitable measurement methods for various engineering applications. Ultimately, this research aims to advance the precision and dependability of deformation measurements within experimental mechanics.

Accurate strain measurement techniques are essential for understanding material behaviour under various loading conditions. Among these, DIC has gained significant attention as a non-contact optical method capable of measuring full-field displacements and strains with high spatial resolution. Recent advancements have focused on improving its accuracy by addressing issues related to calibration, noise reduction, and uncertainty quantification (Pan et al., 2009; Schreier et al., 2009). However, despite its advantages, DIC faces challenges under dynamic conditions and with non-uniform strain fields. On the other hand, FBG sensors, known for their high sensitivity, multiplexing capabilities, and ability to withstand harsh conditions, have demonstrated effectiveness in monitoring localized strain and temperature changes, making them invaluable for applications in structural health monitoring (Campanella et al., 2018). Strain gauges pose a significant challenge to measure mechanical movements at the micro level. Accurate measurement of small resistance changes is critical in the case of strain gauges. Several attempts have been made and are still being made to improve the measurement quality using the Wheatstone bridge because of its very high potential in the field of precision measurement (Kalita et al., 2016). While individual studies have explored the uncertainties and performance of these methods, a comprehensive comparison of their capabilities, particularly under extreme or complex loading scenarios, remains limited. This study aims to fill this gap by conducting a systematic evaluation of these techniques, with a focus on comparative error assessment, dynamic performance, and practical applicability in experimental mechanics. Such an analysis is crucial to advancing measurement reliability and guiding the selection of appropriate techniques for diverse engineering applications.

The principle of strain gauge measurement has been identified as a means to quantify various parameters, including displacement, force, pressure, and acceleration. The strain gauge principle represents about half of all sensor measurement methods (Bethe, 1989). A strain gauge is a device specifically engineered to measure the deformation that a material undergoes when subjected to external forces. It operates on the principle that as the material deforms in response to stress, the strain gauge attached to its surface also experiences deformation, leading to a measurable alteration in its electrical resistance. This relationship between deformation and resistance is defined by the gauge factor, which quantifies the sensitivity of the strain gauge (Hoffmann, 1989). Strain gauges are widely utilized in mechanical testing, structural assessment, and materials science. For instance, they play a crucial role in experimental stress analysis, providing an indirect and reliable measurement of stress distribution across different materials (Dally et al., 1978). Furthermore, resistance strain gauges have been a predominant method for measuring strain, largely attributed to their operational simplicity, cost efficiency, and presumed precision. While generally regarded as accurate instruments, improper application and the neglect of potential error sources remain prevalent issues. Given the impossibility of completely eradicating measurement error, it is imperative to systematically quantify and mitigate such uncertainties to a level that is acceptable for the specific measurement objectives (Montero et al., 2011). While every measurement involves a degree of error and uncertainty, it is impossible to entirely eliminate these inaccuracies; thus, the focus must be on reducing them to an acceptable threshold. Accurately determining measurement uncertainty requires a thorough identification and quantification of the primary error sources. From a practical standpoint, measurement errors and uncertainties should be recognized as integral aspects of the process, often surpassing the significance of the measurement results themselves (Dokoupil, 2017).

FBG sensors consist of periodic changes in the refractive index along an optical fiber, which are produced by exposing the fiber core to a high-intensity optical interference pattern (Hill et al., 1978). Hill and colleagues first introduced this concept in 1978, demonstrating the creation of permanent gratings in germania-doped silica fibers using Argon-ion laser light (Kawasaki et al., 1978). This process led to the reflection of almost all incident light, a phenomenon that came to be known as Hill gratings. Further research found that ultraviolet light, especially at a wavelength of 244 nm, induces photosensitivity more effectively through a two-photon process, resulting in more efficient grating formation. Initially a subject of scientific interest, FBG have since become critical components in optical communication and sensing systems (Hill & Meltz, 1997). Fibers are composed of a core with a diameter ranging from 4 to 9 µm, surrounded by an outer cladding made of pure silica ($SiO_2$) with a diameter of 125 µm. The core exhibits a higher refractive index due to significant doping with germanium. To enhance protection against environmental factors such as water and hydrogen, which can lead to crack propagation and diminish mechanical stability (with the breaking point potentially decreasing from over 30,000 µm/m to as low as 1,000 µm/m), the glass fiber is coated with materials such as acrylate, polyimide, or ORMOCER (modified ceramic) (Kreuzer, 2006).

The fundamental operational principle employed in an FBG sensor system involves observing the variation in the wavelength of the reflected Bragg signal in response to alterations in the measurand, such as strain or temperature. The Bragg wavelength ($\lambda_B$), which represents the resonance condition of the grating, can be described by the following Equation (1) where $\Lambda$ represents the grating period, while n denotes the effective index of the core (Kersey et al., 1997).

$$\lambda_B = 2n\Lambda \tag{1}$$

Mechanical axial strain changes the grating period. It also alters refractive index via the photo-elastic effect. Effective photo-elastic constant ($p_e$) is a function of axial strain. Hereby, tensile strain results in decreasing the refractive index through the photo-elastic effect. So, strain (ε) under constant temperature can be calculated by following Equation (2);

$$\varepsilon = \frac{\Delta\lambda_B}{\lambda_B\,(1-p_e)} \qquad (2)$$

FBG sensors, acknowledged for their superior photosensitivity and optical performance, have emerged as key instruments in structural assessments. Research has extensively evaluated their utility in this domain. For instance, FBG sensors were integrated onto the shear web of a wind turbine blade and employed strain gauges at corresponding locations for comparison (Choi et al., 2012). The findings indicated that the average measurement discrepancies between the FBG sensors and strain gauges were within 2.25%, thereby affirming the FBG sensors' effectiveness for blade evaluation. Similarly, FBG sensors were positioned at the junction of the shear web and beam cap of a blade and performed static testing (Kim et al., 2013). Their results showed minimal variation between FBG sensor measurements, strain gauges, and finite element analysis (FEA), further corroborating the sensors' reliability. Additionally, a distributed FBG sensor system on a prototype blade was utilized to gather data on natural frequencies and strain, which informed improvements in the blade's structural design (Arsenault et al., 2023). The comparative analysis of the original and revised blade designs confirmed the substantial contribution of the sensor data to the enhancement of blade performance (Liu et al., 2020).

DIC, on the other hand, first introduced by researchers from the University of South Carolina in the 1980s, has been systematically refined and extensively utilized across various disciplines over the past thirty years (Peters & Ranson, 1982). The technique is distinguished by its straightforward experimental setup, ease of implementation, and robustness against environmental vibrations and variations in illumination since advanced post-processing algorithms can correct artefacts caused by vibrations. Additionally, high contrast and robust speckle pattern on the surface can enhance capturing image under non-ideal lighting condition to maximize the accuracy of the measurement results. Its adaptability in terms of temporal and spatial resolutions has rendered DIC a highly versatile and effective tool for measuring shape, motion, and deformation in a wide array of materials and structures, across diverse experimental conditions and scales (Dong & Pan, 2017; Isah & Mohamad, 2021; Mata-Falcón et al., 2020). DIC is recognized as a sophisticated and adaptable optical metrology technique for deformation measurement in experimental mechanics. This method entails analysing grayscale digital images of a specimen's surface captured prior to and following deformation to obtain comprehensive deformation data. DIC analysis typically utilizes algorithms based on either subset-based Cross-Correlation (CC) or Sum-Squared Difference (SSD) criteria (Tong, 2005). The precision of DIC measurements is contingent upon several factors, including the implementation of sub-pixel optimization algorithms, the selection of subset shape functions, subset dimensions, sub-pixel intensity interpolation methods, image noise, and lens distortion. Extensive studies have examined the influence of these factors on measurement accuracy (Pan et al., 2008). Experimental studies on small-scale specimens have been utilized to evaluate tensile behaviour, adhesion to substrates, and durability. In contrast, tests on medium- and large-scale specimens, as well as field trials, have provided valuable data on the performance of reinforced structures and have informed the optimization of reinforcement strategies. These studies highlight the critical need to accurately determine mechanical properties essential for effective strengthening design, such as tensile ultimate strength, strain, stiffness, crack spacing, and shear bond strength and displacement. However, traditional measurement devices—such as potentiometers, LVDTs, laser transducers, extensometers, and strain gauges—often face limitations in accurately capturing displacements and strains, particularly in mortar-based composites. Challenges such as cracking, sliding at gripping points, or uneven load distribution may not be adequately detected by these sensors. Furthermore, the reliability of strain and stiffness measurements can be compromised if cracks occur outside the gauge length or if local measurements do not accurately reflect global behaviour. Additionally, traditional sensors may complicate setup preparation, involve high costs, or suffer from damage, which can affect their practicality and reliability (Tekieli et al., 2017).

## 2. Materials and Experimental Setup

The material utilized in this experiment was CYCOM 5575-3. CYCOM 5575 is predominantly favoured for applications within the defence sector. The GFRC material is a modified cyanate ester resin which was subjected to 4 hours curing at 177°C with a cooling rate of 1.8±0.5°C plus 2 hours final curing at 227°C according to ASTM D7028 (ASTM International, 2015). The autoclave pressure was set to 6.9±0.3 bar. The prepregs associated with CYCOM 5575 are available in two primary flow variations, specifically CYCOM 5575-2 and CYCOM 5575-3, and they offer reinforcement options utilizing either quartz or glass fabric (Syensqo, n.d.). The geometry of the specimen as shown Figure 1 and the orientation of the plies were established in accordance with the EN 2747 Type-3 standard (NABau im DIN, 1998).

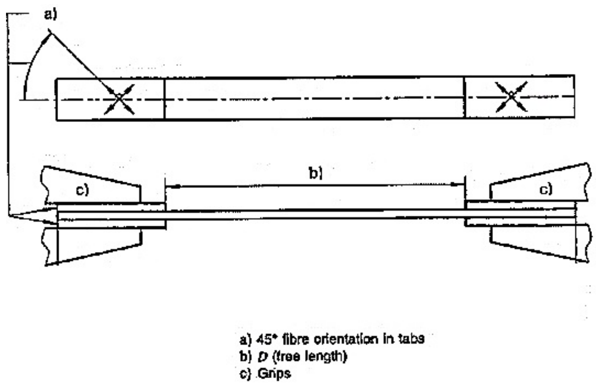


**Figure 1.** Specimen geometry (NABau im DIN, 1998).

EN 2747 Type-3 standard delineates a methodology for evaluating the tensile properties of GFRC designed for aerospace applications. Detailed specifications of the specimen dimensions are provided in Table 1.

**Table 1.** Test specimen dimensions.

| Test Specimen | | | | | | Tab (tapered) | | |
|---|---|---|---|---|---|---|---|---|
| Length (mm) | Width (mm) | Thickness (mm) | # of Plies | Ply Orientation | Material | Length (mm) | Thickness (mm) | Ply Orientation |
| 250±0.5 | 25±0.5 | 2.5±0.5 | 9 | 00 | CYCOM 5575-3 | 50 | 6.75±0.5 | ±450 |

Linear gage measures uniaxial strain along with the applied load. Because of its high accuracy, cost-effective and straightforward instrumentation, strain gages are ideal for basic strain measurements. The strain gauge in a 3-wire configuration, or in other words 1/4 Wheatstone bridge, with a 2V supply voltage chosen for the strain measurement was the CEA-00-125UNA-350 model from Micro-Measurements to gather data from the strain gauge, the MTS FlexDAC 20 (B24 Type) data acquisition system was employed. This system facilitated shunt calibration for the strain gauges, ensuring their proper functionality.

The study employed FBGs FSG-A01-PP0 (Figure 2a), characterized by an effective grating length of 4 mm and a diameter of 155 µm. The initial wavelength recorded was 1558 nm. This sensor utilized a uniform apodised grating modulation, with a 1 mm length Bragg grating inscribed on a single-mode optical fiber. To gather and monitor FBG data during the measurements, the Luna Micron Optics HYPERION si255 (Figure 2b) industrial grade fanless optical sensing interrogator, known for its 1 pm resolution and accuracy, was employed. The FBG sensor was connected to one end of the fiber optic cable via a fixed connection angled physical contact (FC/APC) fiber connector.

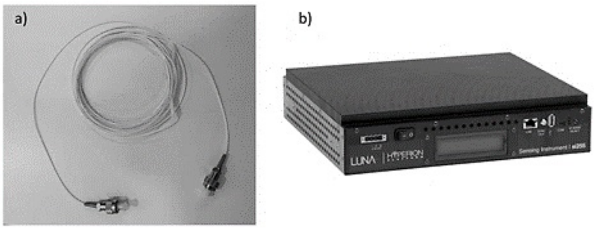


**Figure 2.** (a) FBGs FSG-A01- PP0 sensor and (b) Luna’s Micron Optics HYPERION si255 interrogator.

In the DIC system (Dantec Dynamics GmbH), measurements were taken with high-resolution cameras, each capable of capturing images with a resolution of 4096 (H) x 3000 (V) pixels at Bayer 8-bit depth. The camera sensors feature square pixels with a pixel aspect ratio of 1:1. The tilt of the cameras allowed for the focal planes of both cameras to rotate and overlap within the same region of interest. Illumination was provided by an LED white light source. Camera calibration prior to the test was conducted utilizing a 3D calibration plate that features a defined rectangular dot pattern, characterized by known dot dimensions and spacing at least two different surface elevations. Following the recording of data, image correlation processing was conducted to assess the physical strain derived from the acquired image data. Based on this approach, the facet size was set to 19 pixels and the grid spacing to 3 pixels in order to obtain the best strain values during post-processing of data. In this study, the grid spacing factor and smoothing factor were set to 0.5 and 2.5.

## 3. Static and Fatigue Tests

The specimens were subjected to testing at ambient temperature (23±2°C) and in a controlled laboratory environment with regulated humidity. The test specimens were mounted to an Instron 8801 servo-hydraulic testing machine, which has a load capacity of 100 kN, and were subjected to both static and fatigue loading conditions. The testing was carried out in load-control mode for both types of tests. Prior to the initiation of the tests, one surface of each specimen was prepared for DIC measurement, while the opposite side was instrumented with an FBG sensor and a strain gauge. The FBG sensor was strategically placed at the midpoint of the specimen, with the strain gauge positioned directly above it, aligned along the same axis. KYOWA CC-33A Strain Gauge Adhesive was used for the instrumentation of both strain gage and FBG sensor. Before conducting the static and fatigue tests, a Proportional-Integral-Derivative (PID) settings were established under 1.5 kN alternating loading based on stiffness-based tuning, resulting in a strain of 1000 με on the specimen. At this strain level, all parameters for the strain gauges, FBG sensor, and DIC measurement were fixed. Prior to initiating the testing phase, the camera brightness settings were conducted to enhance illumination, followed by a calibration process aimed at achieving minimal global residuum values. Before calibration process, the camera positions were secured, and all measurements were carried out under the same configuration to isolate any extrinsic parameters that may significantly affect the DIC measurements (Caliskan & Akyuz, 2024). Two images were captured within one second during both static and fatigue loading conditions.

In the static testing phase, the specimen was subjected to a load of 12 kN, implemented in eight distinct steps. Static test was performed with a 20-second ramp time and holding a 20-second to stabilize the sensor output. Following the completion of the static test, a constant amplitude fatigue loading was introduced to the specimen with 0.2 Hz test frequency. This fatigue specimen loading was similarly executed in eight steps, with variations in both the mean and amplitude loads at each stage. The fatigue testing was conducted for 50 cycles at each specified load level. The profiles for both static and fatigue loading are illustrated in Figure 3.

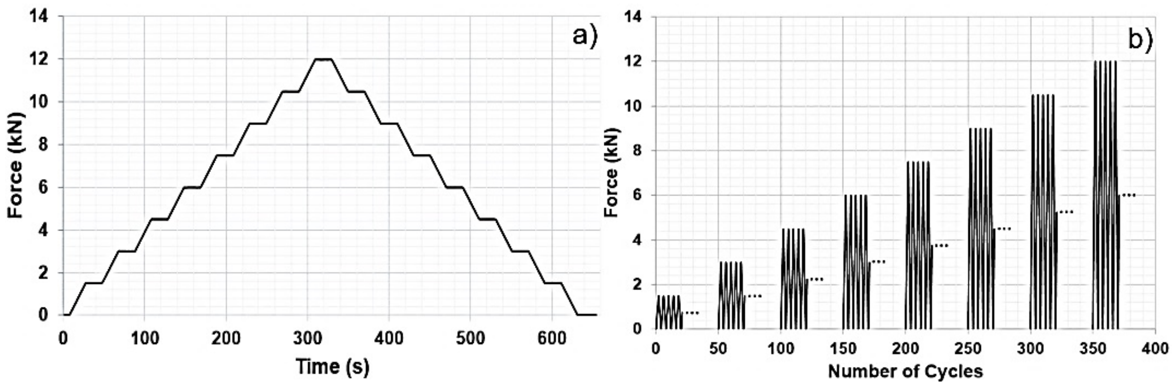


**Figure 3.** (a) Static loading profile and (b) Fatigue loading profile.

Figure 4 depicts the configuration of the experimental apparatus. Strain measurements were obtained from three distinct systems: DIC, FBG sensors, and strain gauges. The strain gauge and DIC were measured at a sampling rate of 2 Hz, while the FBG was at 50 Hz in the static test. On the other hand, the sampling rate for the strain gauge and FBG was 50 Hz, while the sampling rate for the DIC was 2 Hz under fatigue loading at a test frequency of 0.2 Hz. It is important to note that these systems were not synchronized. Nevertheless, efforts were made to initiate recordings from all three systems as concurrently as possible. nCode software was used to generate synchronized data points via down-sampling.

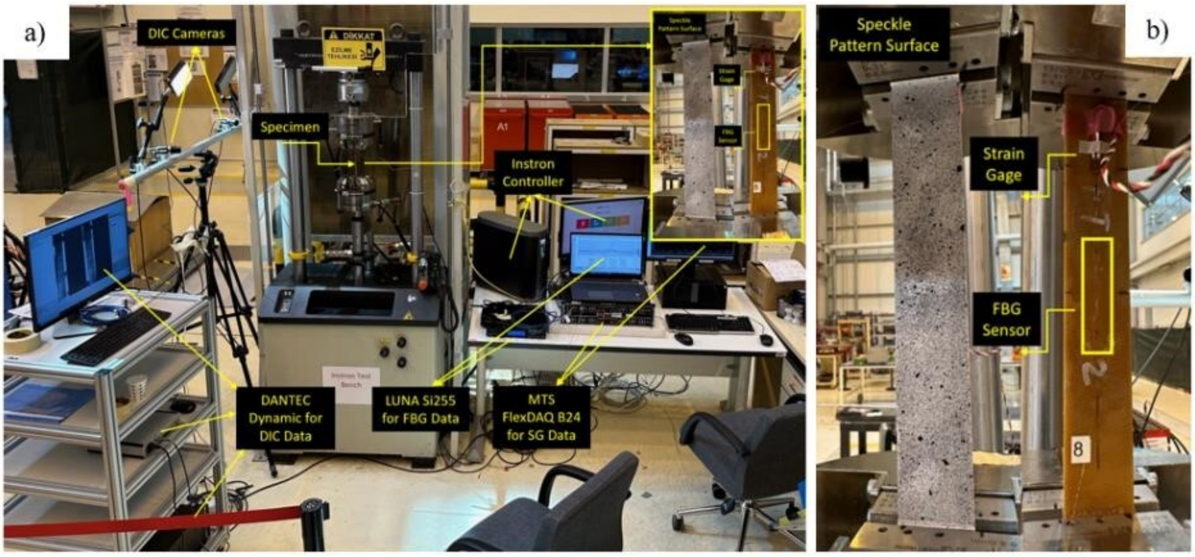


**Figure 4.** (a) Experimental setup and (b) Specimen with sensors.

## 4. Results and Discussion

Strain gage and FBG sensors provide effective real-time monitoring of strain during both static and fatigue testing. In contrast, the images obtained through DIC necessitate post-test analysis. In terms of DIC correlation parameters, the literature indicates no significant correlation between grid spacing and strain values, as these values are derived from the deformation gradient at each data point. Grid spacing decreases below around half of the facet size the facets cease to be independent of each other. Expanding grid spacing decreases data density, which may result in the loss of critical information and the introduction of artificial errors, particularly in regions with high strain variation. Additionally, larger facet sizes tend to distort the accuracy of the strain evaluation due to the inherent smoothing effect. Moreover, the use of larger grid reduction and smoothing factors can lead to over-smoothing in both high and low strain regions, with the smoothing factor exerting a more pronounced effect than the grid reduction factor. The correlation parameters enabled the results to converge to the theoretical strain values. Figure 5 illustrates the graphs depicting strain in relation to time for the results of the static test.

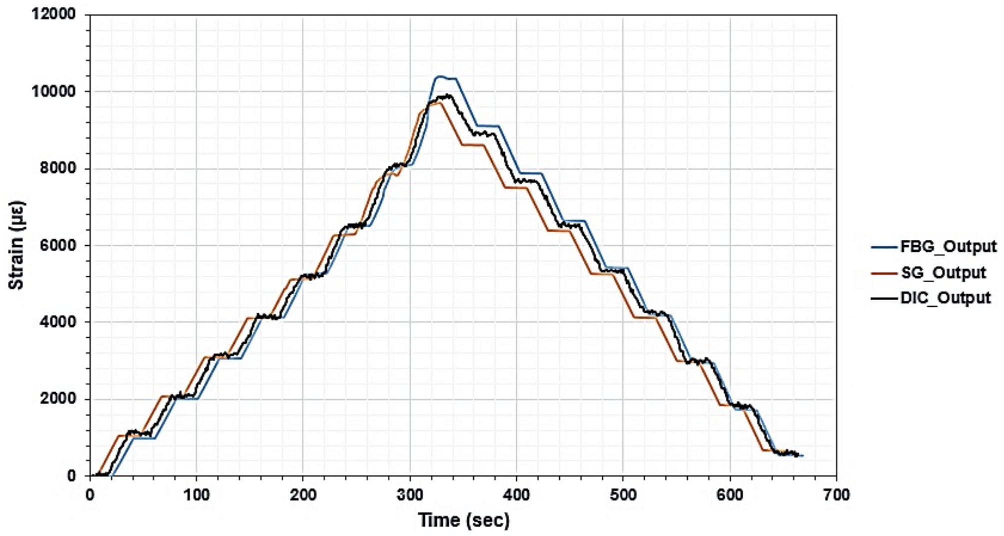


**Figure 5.** Strain vs time graph for static test.

Even though the calibration was performed at 1000 με for all systems, the sensitivity of each measurement system may differ slightly, resulting in variations in response. In addition, factors such as temperature or mechanical noise during calibration may cause small deviations between systems. The static test results demonstrate that DIC having more noise in the measurements. This issue can possibly be resolved by utilizing higher resolution cameras. In order to interpret the result in detail, measured strain values were compared with expected theoretical strain values that is presented in Table 2. The outputs from the three strain measurement techniques reveal comparable results under static loading conditions. The difference between measured strain values for all techniques and theoretical values is maximum 10% until end of Step-6. This difference starts to increase more for last two steps that may be explained by failure of the specimen because the linearity of the measured strain values starts to deviate and nonlinear strain behaviour can be discerned following the fifth loading step. There is a difference of 13% for Step-1 in DIC measurement which could be attributed to post-processing errors.

**Table 2.** Measured strain difference between three different techniques under static load.

| Loading Steps | Step-1 | Step-2 | Step-3 | Step-4 | Step-5 | Step-6 | Step-7 | Step-8 |
|---|---|---|---|---|---|---|---|---|
| Expected Strain (Theoretical, µm/m) | 1,000 | 2,000 | 3,000 | 4,000 | 5,000 | 6,000 | 7,000 | 8,000 |
| Strain Gage (SG) Output (µm/m) | 1,054 | 2,076 | 3,093 | 4,116 | 5,130 | 6,289 | 7,855 | 9,586 |
| FBG Strain Output (µm/m) | 983 | 2,014 | 3,064 | 4,132 | 5,268 | 6,496 | 8,015 | 10,320 |
| DIC Strain Output (µm/m) | 1,128 | 2,088 | 3,143 | 4,149 | 5,202 | 6,501 | 8,036 | 9,784 |
| % Difference (SG vs Expected Strain) | 5 | 4 | 3 | 3 | 3 | 5 | 12 | 20 |
| % Difference (FBG vs Expected Strain) | 2 | 1 | 2 | 3 | 5 | 8 | 15 | 29 |
| % Difference (DIC vs Expected Strain) | 13 | 4 | 5 | 4 | 4 | 8 | 15 | 22 |

In literature, conducted research comparing strain gauge, FBG, and DIC for strain measurements under fatigue loading, especially at high strain levels, has been relatively scarce. Given the variation in sample rates between the DIC measurements and other techniques, it was essential to resample the outputs from the strain gauge and FBG sensor to correspond with the sampling rate established by the DIC. Following this, the strain versus time graphs were generated using the resampled results derived from of strain gage and FBG. The results of the fatigue tests are illustrated in Figure 6.

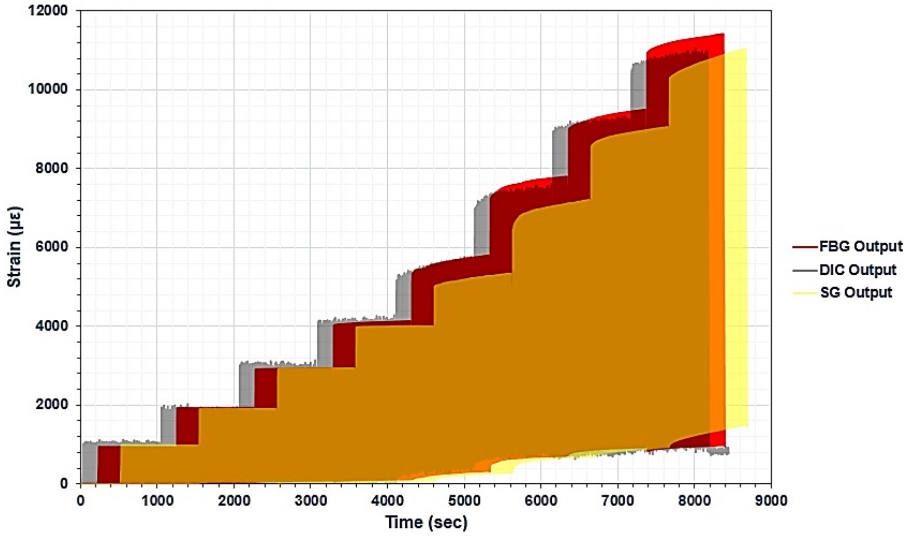


**Figure 6.** Strain vs time graph for fatigue test.

The results of the fatigue test indicate that noise in the DIC measurements persists under fatigue loading, potentially attributable to the resolution of the cameras used. Furthermore, it can be observed that the linearity of the measured strain values begins to diverge following the fourth loading step. It can also be stated that the three strain measurement techniques yield comparable results in fatigue testing up to the point of maximum fatigue loading. At Step-4, the observed strain values exhibit a close proximity to each other as well as to the theoretical value. The measured strain values from strain gauges, FBG, and DIC exhibit a greater deviation from theoretical values under fatigue loading compared to the discrepancies noted during static testing, particularly in the last three steps of the assessment. The comparison of the measured strain values against the theoretical values is thoroughly outlined in Table 3.

**Table 3.** Measured strain difference between three different techniques under fatigue load.

| Loading Steps | Step-1 | Step-2 | Step-3 | Step-4 | Step-5 | Step-6 | Step-7 | Step-8 |
|---|---|---|---|---|---|---|---|---|
| Expected Delta-Strain (Theoretical, μm/m) | 1,000 | 2,000 | 3,000 | 4,000 | 5,000 | 6,000 | 7,000 | 8,000 |
| Strain Gage (SG) Delta-Output (μm/m) | 982 | 1,908 | 2,917 | 3,981 | 5,178 | 6,834 | 8,826 | 10,666 |
| FBG Delta-Strain Output (μm/m) | 940 | 1,930 | 2,909 | 4,013 | 5,557 | 7,509 | 9,236 | 11,176 |
| DIC Delta-Strain Output (μm/m) | 1,022 | 1,893 | 2,936 | 4,079 | 5,448 | 7,225 | 9,088 | 10,743 |
| % Difference (SG vs Expected Strain) | 2 | 5 | 3 | 0 | 4 | 14 | 26 | 33 |
| % Difference (FBG vs Expected Strain) | 6 | 4 | 3 | 0 | 11 | 25 | 32 | 40 |
| % Difference (DIC vs Expected Strain) | 2 | 5 | 2 | 2 | 9 | 20 | 30 | 34 |

Adhesives used in strain gauges usually begin to degrade when subjected to strain levels between 3,000 and 5,000 µm/m, because the mechanical stress can exceed their bonding and elastic limits. This degradation can lead to a weakening of the bond between the strain gauge and the specimen surface, causing inaccuracies and variability in strain readings. Furthermore, over time - especially under cyclic loading or in extreme environmental conditions such as high temperatures and humidity - the performance of the adhesive can degrade significantly, ultimately leading to complete bond failure. According to the results of the study, specimen deterioration such as starting fiber breakage and adhesive slippage was observed after a strain value of 4,000 µm/m under alternating loading while the variation in data is consistent for all measurements. However, since the results of the non-contact measurement method DIC show the same trend in terms of specimen degradation as the FBG and strain gauge results, it can be evaluated that specimen degradation is a more dominant effect compared to adhesive degradation.

## 5. Conclusion

This study attempts to address the shortcomings by conducting a systematic evaluation of FBG, DIC and strain gage measurement techniques, focusing on their performance, comparative error assessment, and practical usability. In doing so, it provides valuable information to guide the selection of the most appropriate measurement methods for different engineering applications. Ultimately, this research is aimed at improving the accuracy and reliability of strain measurements in experimental mechanics. The following conclusions can be reached from this study. The same types of adhesives are applicable for the mounting of both strain gauges and FBG sensors. The DIC measurement exhibit higher level of fluctuation compared to strain gage and FBG sensor under static and fatigue loading. This research indicates that strain gauges, FBG sensors, and DIC show a maximum ten 10% variation in strain values from theoretical estimates, applicable for strains reaching up to 6,000 µm/m under static loading. The results of strain measurement utilizing strain gages, FBG, and DIC techniques exhibit a high degree of comparability when subjected to fatigue loading, specifically up to 4,000 µm/m.

## Conflict of Interest

The corresponding author confirms on behalf of all authors that there have been no involvements that might raise the question of bias in the work.

## Author Contributions

The corresponding author contributed to the FBG section, and the secondary author contributed to the DIC section.

## Funding

This research received no specific grant from any funding agency in the public, commercial, or not-for-profit sectors.

## Acknowledgments

Authors acknowledge Turkish Aerospace Industries.

## Ethical Statements

The corresponding author testify on behalf of all co-authors that our article submitted followed ethical principles in publishing.

## Data and Code Availability

The authors confirm that the data supporting the findings of this study are available within the article.

## Supplementary Materials

The authors confirm that the data supporting the findings of this study are available within the article and its supplementary materials.

## References

Arsenault, T. J., Achuthan, A., Marzocca, P., Grappasonni, C., & Coppotelli, G. (2013). Development of a FBG-based distributed strain sensor system for wind turbine structural health monitoring. *Smart Materials and Structures*, *22*(7), 075027. https://doi.org/10.1088/0964-1726/22/7/075027

ASTM International. (2015). *ASTM D7028-07: Standard test method for glass transition temperature (DMA Tg) of polymer matrix composites by dynamic mechanical analysis (DMA).* ASTM International.

Bethe, K. (1989). The scope of the strain gage principle. In *Proceedings of COMPEURO 89: VLSI and computer peripherals.* COMPEURO 89 (pp. 3–31). IEEE.

Caliskan, S., & Akyuz, H. (2024). Investigation of the speckle pattern effect for displacement assessments by DIC. *Journal of Intelligent Manufacturing and Special Equipment*.

Campanella, C. E., Cuccovillo, A., Campanella, C., Yurt, A., & Passaro, V. M. (2018). Fibre Bragg grating based strain sensors: Review of technology and applications. *Sensors, 18*(9), 3115. https://doi.org/10.3390/s18093115

Choi, K. S., Huh, Y. H., Kwon, I. B., & Yoon, D. J. (2012). A tip deflection calculation method for a wind turbine blade using temperature compensated FBG sensors. *Smart Materials and Structures, 21*(2), 025008. https://doi.org/10.1088/0964-1726/21/2/025008

Cycom 5575. (n.d.). *Syensqo*. https://www.syensqo.com/en/product/cycom-5575-0

Dally, J. W., Riley, W. F., & Kobayashi, A. S. (1978). *Experimental stress analysis*. McGraw-Hill.

DIN Deutsches Institut für Normung. (1998). *DIN EN 2747: Glass fiber-reinforced plastics – Tensile test*. DIN.

Dokoupil, P. (2017). *Determination of measurement uncertainty of strain and stress using strain gages*. *Sborník vědeckých prací Vysoké školy báňské - Technické univerzity Ostrava. 63*(1), 9-23, https://doi.org/10.22223/tr.2017-1/2023

Dong, Y. L., & Pan, B. (2017). A review of speckle pattern fabrication and assessment for digital image correlation. *Experimental Mechanics, 57,* 1161–1181. https://doi.org/10.1007/s11340-017-0283-1

Hill, K. O., & Meltz, G. (1997). Fiber Bragg grating technology fundamentals and overview. *Journal of Lightwave Technology, 15*(8), 1263–1276. https://doi.org/10.1109/50.618320

Hill, K. O., Fujii, Y., Johnson, D. C., & Kawasaki, B. S. (1978). Photosensitivity in optical fiber waveguides: Application to reflection filter fabrication. *Applied Physics Letters, 32*(10), 647–649. https://doi.org/10.1063/1.89881

Hoffmann, K. (1989). *An introduction to measurements using strain gages*. Hottinger Baldwin Messtechnik.

Isah, B. W., & Mohamad, H. (2021). Surface-mounted bare and packaged fiber Bragg grating sensors for measuring rock strain in uniaxial testing. *Sensors, 21*(9), 2926. https://doi.org/10.3390/s21092926

Kalita, K., Das, N., Boruah, P. K., & Sarma, U. (2016). Design and uncertainty evaluation of a strain measurement system. *MAPAN, 31*, 17–24. https://doi.org/10.1007/s12647-015-0155-z

Kawasaki, B. S., Hill, K. O., Johnson, D. C., & Fujii, Y. (1978). Narrow-band Bragg reflectors in optical fibers. *Optics Letters, 3*(2), 66–68. https://doi.org/10.1364/OL.3.000066

Kersey, A. D., Davis, M. A., Patrick, H. J., LeBlanc, M., Koo, K. P., Askins, C. G., … Friebele, E. J. (1997). Fiber grating sensors. *Journal of Lightwave Technology, 15*(8), 1442–1463. https://doi.org/10.1109/50.618377

Kim, S., Kang, W., Jeong, M., Lee, I., & Kwon, I. (2013). Deflection estimation of a wind turbine blade using FBG sensors embedded in the blade bonding line. *Smart Materials and Structures*, *22*(12), 125004. https://doi.org/10.1088/0964-1726/22/12/125004

Kreuzer, M. (2006). *Strain measurement with fiber Bragg grating sensors*. HBM.

Liu, Z., Liu, X., Zhu, S. P., Zhu, P., Liu, W., Correia, J. A., & De Jesus, A. M. (2020). Reliability assessment of measurement accuracy for FBG sensors used in structural tests of wind turbine blades based on strain transfer laws. *Engineering Failure Analysis, 112,* 104506. https://doi.org/10.1016/j.engfailanal.2020.104506

Mata-Falcón, J., Haefliger, S., Lee, M., Galkovski, T., & Gehri, N. (2020). Combined application of distributed fibre optical and digital image correlation measurements to structural concrete experiments. *Engineering Structures, 225*, 111309. https://doi.org/10.1016/j.engstruct.2020.111309

Montero, W., Farag, R., Diaz, V., Ramirez, M., & Boada, B. L. (2011). Uncertainties associated with strain-measuring systems using resistance strain gauges. *Journal of Strain Analysis for Engineering Design*, *46*(1), 1–13. https://doi.org/10.1243/03093247JSA661

Pan, B., Qian, K., Xie, H., & Asundi, A. (2009). Two-dimensional digital image correlation for in-plane displacement and strain measurement: A review. *Measurement Science and Technology, 20*(6), 062001. https://doi.org/10.1088/0957-0233/20/6/062001

Pan, B., Xie, H., Wang, Z., Qian, K., & Wang, Z. (2008). Study on subset size selection in digital image correlation for speckle patterns. *Optics Express, 16*(10), 7037–7048. https://doi.org/10.1364/OE.16.007037

Peters, W. H., & Ranson, W. F. (1982). Digital imaging techniques in experimental stress analysis. *Optical Engineering, 21*(3), 427–431. https://doi.org/10.1117/12.7972925

Schreier, H., Orteu, J. J., & Sutton, M. A. (2009). *Image correlation for shape, motion and deformation measurements: Basic concepts, theory and applications*. Springer. https://doi.org/10.1007/978-0-387-78747-3

Tekieli, M., De Santis, S., de Felice, G., Kwiecień, A., & Roscini, F. (2017). Application of digital image correlation to composite reinforcements testing. *Composite Structures*, *160*, 670–688. https://doi.org/10.1016/j.compstruct.2016.10.096

Tong, W. (2005). An evaluation of digital image correlation criteria for strain mapping applications. *Strain, 41*(4), 167–175. https://doi.org/10.1111/j.1475-1305.2005.00227.x